Influence of the 26 degrees N RAPID-MOCHA Array and Florida Current Cable Observations on the ECCO-GODAE State Estimate

Citation: Baehr, Johanna. "Influence of the 26°N RAPID–MOCHA Array and Florida Current Cable Observations on the ECCO–GODAE State Estimate." J. Phys. Oceanogr. 40.5 (2011) : 865-879. Copyright c2010 American Meteorological Society

As Published: http://dx.doi.org/10.1175/2009jpo4118.1

Publisher: American Meteorological Society

Persistent URL: http://hdl.handle.net/1721.1/64812

Version: Final published version: final published article, as it appeared in a journal, conference proceedings, or other formally published context

Influence of the 26°N RAPID–MOCHA Array and Florida Current Cable Observations on the ECCO–GODAE State Estimate

JOHANNA BAEHR*

Department of Earth, Atmospheric, and Planetary Sciences, Massachusetts Institute of Technology, Cambridge, Massachusetts

(Manuscript received 12 August 2008, in final form 21 December 2009)

ABSTRACT

The incorporation of local temperature and salinity observations from the Rapid Climate Change–Meridional Overturning Circulation and Heatflux Array (RAPID–MOCHA), as well as the cable estimates of volume transport in the Florida Current (FC), is tested in the Estimating the Circulation and Climate of the Ocean–Global Ocean Data Assimilation Experiment (ECCO–GODAE) estimation system for their impact on the estimate of the meridional overturning circulation (MOC) and the meridional heat transport in the Atlantic. An experimental setup covering the first deployment period of RAPID–MOCHA from March 2004 to March 2005 is used to test different strategies for incorporating these datasets. Incorporating both monthly means of the FC data and monthly means of the RAPID–MOCHA temperature and salinity measurements at the eastern and western boundaries of the basin as an observational constraint in a 1-yr experiment results in an adjustment to the reference estimate, which does not include these datasets, of approximately 1 Sv (1 Sv $\equiv$ 10^6 m^3 s^{-1}) in the MOC at 26°N and the adjacent latitudes (approximately $\pm$15°), with a larger northward branch of the MOC above 1000 m, compensated by a larger flow in the southward branch of the MOC between approximately 2000 and 3000 m. The meridional heat transport from 26°N to near 40°N is approximately 0.05 PW larger than in the reference experiment.

1. Introduction

Oceanic state estimates bring a general circulation model to consistency with a multitude of observations. Dynamically consistent oceanic state estimates have recently become available [e.g., from the Estimating the Circulation and Climate of the Ocean (ECCO) project], using a general circulation model [the Massachusetts Institute of Technology general circulation model (MITgcm); Marshall et al. 1997]. They cover the time span of the altimetric record beginning in 1992 (Wunsch and Heimbach 2006) or go back to the beginning of the National Centers for Environmental Prediction–National Center for Atmospheric Research (NCEP–NCAR) reanalysis period in 1952 (Köhl and Stammer 2008). Within such a dynamically consistent framework, any oceanic quantity, including integrated quantities such as meridional heat and mass transports, can be derived from the full three-dimensional ocean state, which provides a continuous observation-based estimate of that quantity. Such an observation-based and dynamically consistent estimate of integrated quantities is of special importance as these integrated quantities are difficult to observe directly.

Until recently, most studies of the global oceanic heat and mass transports had to rely on occasional hydrographic sections (Hall and Bryden 1982; Roemmich and Wunsch 1985; Bryden et al. 2005; Ganachaud and Wunsch 2000; Longworth and Bryden 2007); however, sparse sampling (once every few years or decades) of these transects represents a time series with serious aliasing problems, complicating the interpretation of estimated variability or trends considerably (Wunsch and Heimbach 2006; Baehr et al. 2008). Although the Argo array provides a much denser database, it needs to be synthesized in an oceanic state estimate to allow for an estimate of heat and mass transports. Forget et al. (2008a,b) suggest that Argo profiles allow improved estimates of heat and mass transports when synthesized in such a state estimate.

* Current affiliation: Institute of Oceanography, Klima Campus, University of Hamburg, Hamburg, Germany.

Corresponding author address: Johanna Baehr, Institute of Oceanography, Klima Campus, University of Hamburg, Grindelberg 5, 20144 Hamburg, Germany.
E-mail: johanna.baehr@zmaw.de

DOI: 10.1175/2009JPO4118.1

In March 2004, a monitoring system was deployed to provide a continuous estimate of the zonally integrated meridional mass transport at 26.5°N in the Atlantic (Marotzke et al. 2002; Cunningham et al. 2007; Kanzow et al. 2007). This Rapid Climate Change–Meridional Overturning Circulation and Heatflux Array (RAPID–MOCHA) is based on continuous monitoring of the density at the eastern and western boundaries of a zonal section, based on a conceptual study by Marotzke et al. (1999), suggesting that the meridional overturning circulation (MOC) could be continuously monitored using such measurements. The RAPID–MOCHA consists of profiles of density at the western and eastern boundaries as well as on both sides of the Mid-Atlantic Ridge (MAR; Marotzke et al. 2002; Rayner 2005). To compute the MOC, the observations of the vertical density profiles at the boundaries are combined with the Florida Current (FC) cable measurements (Baringer and Larsen 2001) and an estimate of the wind-driven Ekman transport based on scatterometer wind measurements (Graf et al. 1998).

Although the observations of the RAPID–MOCHA and the Florida Current provide a local estimate of the MOC at 26°N in the Atlantic, they do not allow for immediate conclusions about adjacent altitudes or even basin-scale variations in the MOC. Incorporating these observations into a dynamically consistent oceanic state estimate is therefore a useful addition to the analysis of the global observing system. Although the ECCO–Global Ocean Data Assimilation Experiment (ECCO–GODAE) project includes most of the global datasets in the observing system, it does not yet incorporate local mooring transport estimates. The present study investigates the best means to incorporate and weight these data in the least squares methodology of ECCO–GODAE and draws some inferences about their likely impact.

Here, we will incorporate both the Florida Current and RAPID–MOCHA observations into 1-yr optimizations of the ECCO–GODAE oceanic state estimate. With 1-yr optimizations, we will focus on the first deployment period of the RAPID–MOCHA (March 2004–March 2005). These 1-yr optimizations provide a computationally feasible setup for explorative studies, allowing the conduct of a series of experiments. Note that the baroclinic response time in the ocean at these latitudes is on the order of a decade. Therefore, we do not expect a large adjustment at 26°N or even in the North Atlantic circulation and its variability because of the spatial and temporal restriction of the data. The main objective of this study is to guide the incorporation of integrated transport measurements such as the Florida Current data and moored temperature and salinity observations such as the RAPID–MOCHA data into the full ECCO–GODAE estimate. The incorporation of the FC and RAPID–MOCHA data into the dynamically consistent ECCO–GODAE solution in turn gives the prospect of an enhanced understanding of the meridional transport and its variability at both 26°N and in the whole North Atlantic.

The paper is structured as follows: section 2 provides an overview of the model and observations used in this study. Section 3 presents the results of the numerical experiments, which are discussed in section 4.

2. Method

a. ECCO–GODAE framework and 1-yr experimental setup

We use the quasi-global ocean state estimate ECCO–GODAE setup. ECCO–GODAE aims to bring the MITgcm (Marshall et al. 1997) to consistency with as many observations as practical on a global level within estimated uncertainties. The reduction of the quadratic model versus data misfit (the so-called cost function) is achieved via a gradient descent method. The gradient of the cost function with respect to initial conditions and time-varying air–sea fluxes is computed via the adjoint of the MITgcm (Marotzke et al. 1999; Heimbach et al. 2005). The code for the MITgcm's adjoint has been derived by means of the Transformation of Algorithms in FORTRAN automatic differentiation tool (Giering and Kaminski 1998). Very briefly, the cost function is reduced as follows: (i) it starts from a model setup with best estimate initial conditions and forcing; (ii) the model setup is then run forward/backward over a specific number of iterations while making adjustments to the initial conditions and forcing to reduce disagreement with the multitude of observations; and (iii) it is finally freely run forward in time with the adjusted initial conditions and forcings after the solution has converged or is close to convergence, thus producing a solution completely consistent with the model equations.

The ECCO–GODAE setup covers the World Ocean between 80°N and 80°S, excluding the Arctic, at 1° horizontal resolution with 23 vertical levels. We employ a setup version 2 of the ECCO–GODAE state estimation at MIT and Atmospheric and Environmental Research (AER), on which previous results describing 26°N are based as well (e.g., Wunsch and Heimbach 2006; Baehr et al. 2009). An overview of the method and the datasets employed in ECCO–GODAE is provided in Wunsch and Heimbach (2007; for an overall account of efforts within the ECCO Consortium, see online at http://www.ecco-group.org).

Here, we use an experimental subset of the full ECCO–GODAE state estimate. It differs from the full

ECCO–GODAE setup in the reduction of the optimization period from 15 yr to 18 months and an increase in the vertical resolution (from 23 to 50 levels). This experimental setup is similar to the one used in Forget (2010); it includes the same observations as the full ECCO–GODAE state estimate: for example, the temperature and salinity profiles from the Argo floats since 2004 (for a complete list, see, e.g., Wunsch and Heimbach 2006). In the experimental setup, we use the Ocean Comprehensive Atlas (OCCA) of Forget (2010) as initial condition and climatological constraint, and 6-hourly atmospheric state variables from the NCEP–NCAR reanalysis are used as a starting point for the atmospheric boundary conditions. This experimental setup is overall considerably closer to the observations than the ECCO–GODAE estimate, because the initial conditions are more efficient controls over the shorter period. On the limited time scale of 1 yr, the experimental setup allows us to investigate the added value of the RAPID–MOCHA and FC observations to the existing observing system more realistically than a setup initialized by ECCO–GODAE fields. This difference to the full ECCO–GODAE state estimate, however, limits the inferences about the extent to which the present results can be directly applied to the much longer duration ECCO–GODAE estimate.

The experimental setup covers a period of 18 months from 1 January 2004 to 30 June 2005. Of that period, we analyze the first deployment period of the RAPID–MOCHA from 29 March 2004 to 31 March 2005: that is, we disregard the first 3 months and the last 3 months of the optimization. Therefore, we will refer to this experimental configuration as the 1-yr setup. Prior to iteration one, the 1-yr setup has been spun up for 6 months. Subsequently, a ''reference'' experiment has been conducted for 10 iterations, including the full suite of observations as constraints but excluding both the FC and the RAPID–MOCHA data. After 10 iterations the solution is not fully converged but is largely adjusted to the initial conditions. Note observations were as such not excluded for the first 10 iterations; however, the adjustment to the initial conditions is dominant over the adjustment to the observations for the first few iterations. The FC and RAPID–MOCHA data are included from iteration 11 onward. For the experiments including the FC and RAPID–MOCHA data, we perform another 5–10 iterations, the exact number of iterations depending on the experiment. All experiments were run until the reduction in the cost function for the respective dataset was less than 4% from one iteration to the next. For comparison, the same number of iterations was carried out for the reference experiment without including these data to exclude the effect of adjustment to the data solely because of a larger number of iterations.

Limiting the present analysis to a 1-yr period is mostly constrained by the availability of the RAPID–MOCHA data. Additionally, the 1-yr setup provides a computationally less expensive setup than the full ECCO–GODAE setup. Not only is the integration time much shorter, but also the number of iterations needed to converge toward certain data is considerably smaller in the 1-yr setup. For the reference experiment to reduce the change in the total cost function to 2% from one iteration to the next, 25 interactions are needed. Although this 1-yr setup allows for multiple experiments, it also limits the interpretation of the results, because, on these time scales, mostly local adjustments to the data can be expected. Any temporal variability requiring large-scale adjustment is likely to involve time scales of years or decades.

The geographical setup at 26°N in the Atlantic is identical in both the 1-yr setup and ECCO–GODAE: despite its 1° horizontal resolution, the Bahamas are represented; the Straits of Florida have a realistic depth and shape but span nearly 400 km compared with approximately 100 km width in the real ocean. These extended Straits of Florida prevent the resolution of the western boundary continental slope: to the east of the Bahamas the ocean basin is bounded by a vertical wall. Most of the northward transport goes through the Straits of Florida; the Antilles Current has a time mean between 1 and 2 Sv (1 Sv $\equiv 10^6$ m^3 s^{-1}; not shown), which is smaller than the 6 Sv observed by Meinen et al. (2004). The standard deviation of the Antilles Current is approximately 2.5 Sv for ECCO–GODAE compared to 3 Sv observed by Meinen et al. (2004).

b. Observations

The FC is observed by measuring the flow-induced voltage in a telephone cable, which runs between Florida and the Bahamas along the sea floor (Larsen 1985). This observing system is maintained by the U.S. National Oceanic and Atmospheric Administration and has provided daily estimates of Gulf Stream transport for over 20 years now (Baringer and Larsen 2001). We use daily-mean values with an associated observation error of 2 Sv root-mean-square error (C. S. Meinen 2008, personal communication).

The RAPID–MOCHA provides continuous observations of the density profile at the eastern and western boundaries at 26.5°N of the Atlantic (Marotzke et al. 2002; Cunningham et al. 2007; Kanzow et al. 2007). Densities are derived from sensors attached to moorings measuring temperature, salinity, and pressure at a temporal resolution of 15 min. Here, we use the temperature and salinity (not pressure) data from the western and eastern boundaries, interpolated on a 20-dbar vertical grid

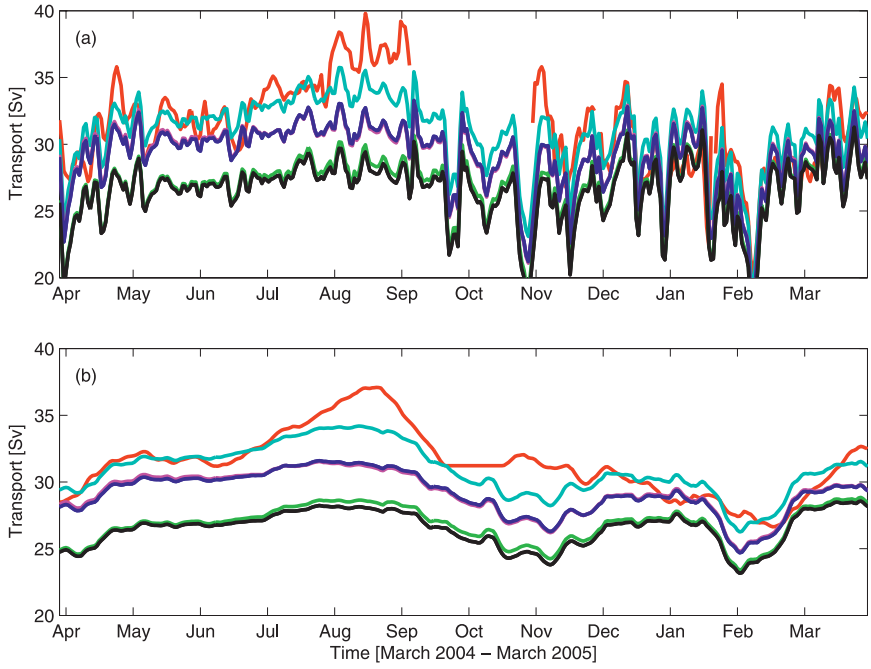

FIG. 1. Time series of FC (Sv) for the first deployment period of RAPID–MOCHA: cable observations (red line), 1-yr optimization reference experiment (black line), daily FC experiment (cyan line), monthly FC experiment (blue line), experiment with reference experiment wind stress (magenta line), and experiment with optimized wind stress (green line). Shown are (a) daily values and (b) smoothed with a running mean of two months.

(Kanzow et al. 2007). Given the model's limited horizontal resolution, we use merged profiles from Kanzow et al. (2007) for both the western and eastern boundaries. For the western boundary, density data from 24 depth levels between 100 and 4820 dbar distributed among three moorings on the steep continental rise east of the Bahamas are used. For the eastern boundary, profile density data from 23 depth levels between 550 and 4930 dbar distributed among six moorings between the base of the 1000-km-wide eastern continental slope and the Moroccan shelf are merged. When including the RAPID–MOCHA data, we generally use temperature and salinity as a constraint, with one exception, where we use the meridional (geostrophic) midocean transport estimate by Cunningham et al. (2007): that is, the transport derived from the merged density profiles of RAPID–MOCHA.

3. Optimizations

To investigate the impact of the Florida Current cable observations and the RAPID–MOCHA data, we initially incorporate them separately into 1-yr experiments. Subsequently, we investigate the combined incorporation of the two datasets into 1-yr experiments.

a. Florida Current

The observed Florida Current transport between the end of March 2004 and the end of March 2005 has a time-mean value of 31.7 Sv (Fig. 1). The reference experiment shows a smaller time-mean value of 27.3 Sv. Over this 1-yr period, the variability in the observed FC of 3.3 Sv standard deviations is larger than the standard deviation of 2.4 Sv in the reference experiment; however, the high-frequency variability in the FC is reproduced quite realistically in the reference experiment. This agreement between observations and reference experiments originates mostly from the incorporation of wind stress observations. Note that for the same period the full ECCO–GODAE estimate has a time-mean value of 26.5 Sv with a standard deviation of 2.9 Sv (Baehr et al. 2007). As in the 1-yr reference solution, the full ECCO–GODAE estimate also reproduces the high-frequency variability (i.e., the Ekman transport across 26°N, quite realistically; Baehr et al. 2007); however, in the full ECCO–GODAE estimate, this is mostly mirrored in a realistic reproduction of the high-frequency MOC variability (Baehr et al. 2007).

To test the influence of the incorporation of the transport integrated over the Straits of Florida across 26°N on the solution, we initially upweight the FC transport

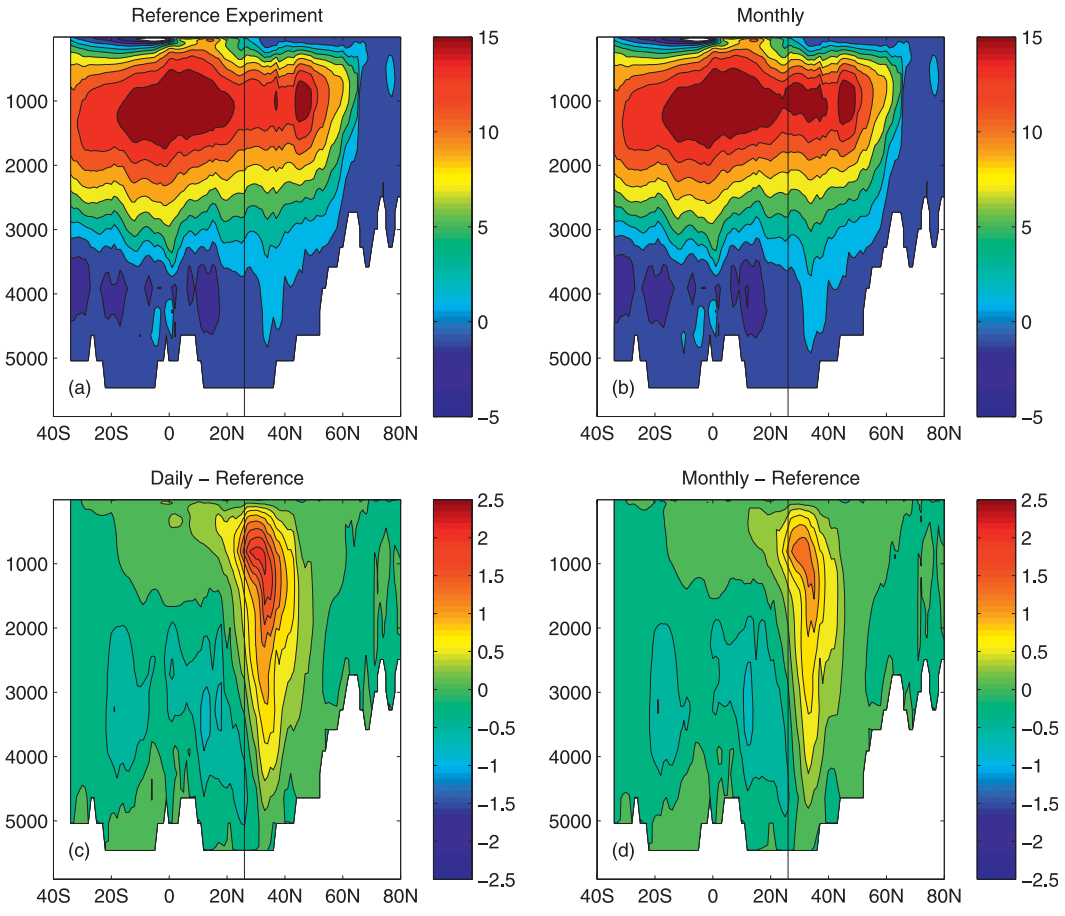

FIG. 2. Time-mean Atlantic MOC (Sv; over first deployment period of RAPID–MOCHA) for (a) reference experiment and (b) monthly FC experiment. Difference from reference experiment for (c) daily FC experiment and (d) monthly FC experiment.

artificially. First, in the "daily FC" experiment, we use daily-mean values of the observed FC transport with an observation error of 2 Sv (C. S. Meinen et al. 2008, personal communication) upweighted by a factor 100, increasing the contribution of the FC misfit to the total cost function from 1% to 10%. This daily FC experiment results in a larger time-mean value after five iterations (27.3–30.9 Sv; Fig. 1). In this upweighted daily FC experiment, the optimization works on the time-mean value, while the short-term variability is barely affected (2.4–2.7 Sv). To reduce the high-frequency variability to which the optimization is not sensitive, we average the data to monthly means ("monthly FC") but preserve a daily time series. In turn, we reduce the observation error to 0.5 Sv (C. S. Meinen et al. 2008, personal communication), resulting in a contribution of the FC misfit of approximately 5% to the total cost function. With no additional upweighting, the time-mean value is larger compared to the reference experiment to 29.1 Sv with a standard deviation of 2.5 Sv after five iterations (Fig. 1).

The larger FC transport at 26°N translates into a larger northward transport in the top 1000 m (i.e., the depth of the Florida Straits in the model) for latitudes between just south of 26°N and approximately 35°N (Fig. 2). This intensified northward transport is largely confined to the western boundary (Fig. 3). The vertical structure of this larger transport is similar for the upweighted daily values and the monthly-mean values, although different in magnitude (Fig. 2). The larger northward transport is all recirculated southward in the western part of the basin to approximately 35°N (Fig. 3), and a corresponding cyclonic recirculation anomaly develops north of this cell. As for the vertical structure, the zonal structure of this larger transport is similar for the daily FC experiment and the monthly FC experiment, although different in magnitude (Fig. 3).

To understand whether the larger time-mean FC transport in the monthly FC experiment originates from the differences in the forcing or the initial conditions, we perform two sensitivity experiments: in a single forward

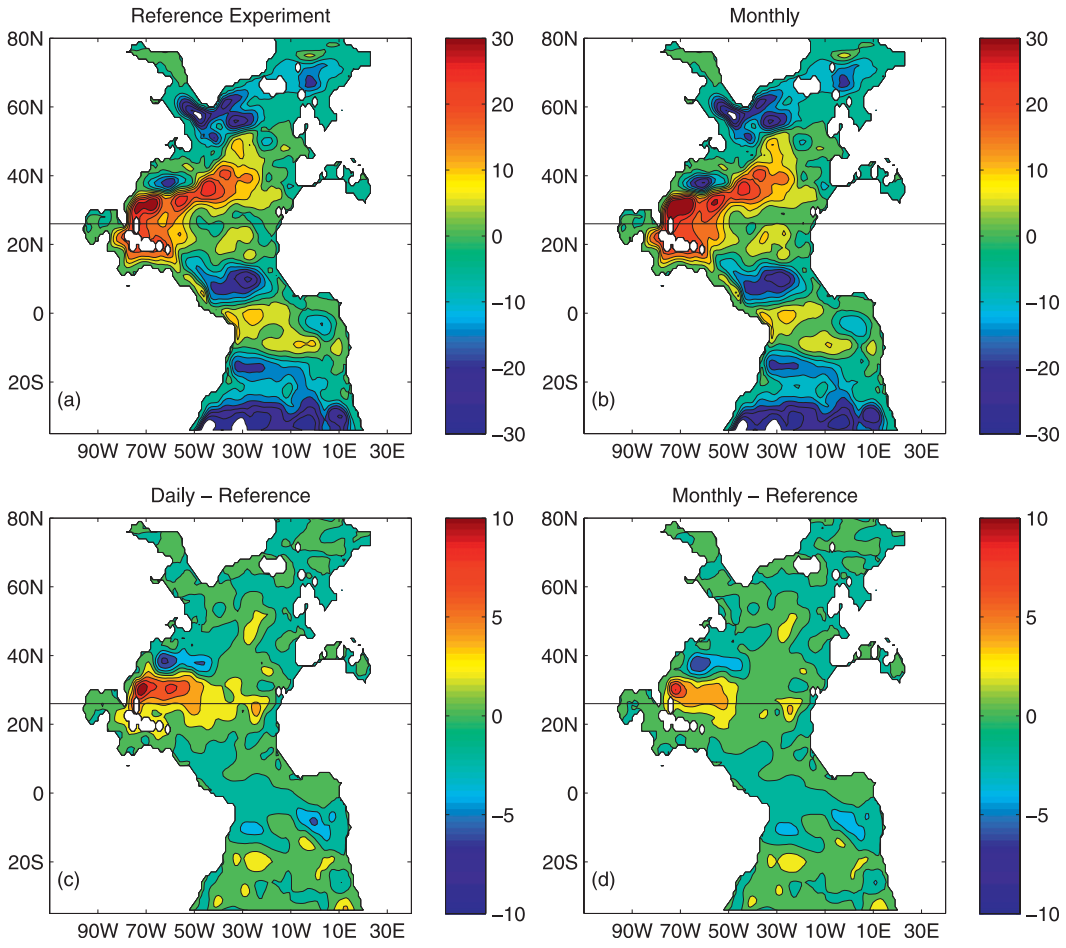

FIG. 3. Time-mean vertically and zonally (cumulative) integrated meridional volume transport (Sv; also referred to as barotropic streamfunction) in the Atlantic over first deployment period of RAPID–MOCHA for (a) reference experiment and (b) monthly FC experiment. Difference from reference experiment for (c) daily FC experiment and (d) monthly FC experiment.

run, we force (i) the reference experiment with the adjusted wind stress from the FC monthly experiment and (ii) the FC monthly experiment with the adjusted wind stress from the reference experiment. Using (i), the adjusted wind stress from the FC monthly experiment results in a similar time mean and variability as the reference experiment (Fig. 1). Using (ii), the wind stress from the reference experiment results in a similar FC variability and time-mean strength as the FC monthly experiment (Fig. 1). Therefore, the main impact on the solution comes from adjustments to the initial conditions. Note that this is likely to change for state estimates performed over longer periods of times.

In our test, the optimization appears not sensitive to the intensification of the FC transport in summer, although it is clearly impossible to infer a robust adjustment to the seasonal cycle from these 1-yr experiments (Fig. 1). Anderson and Corry (1985) suggest that the meridional component of the wind stress is responsible for the summer intensification, while the zonal component of the wind stress is primarily responsible for the mean flow, assuming that the baroclinic response times at midlatitudes is on the order of one decade (Veronis and Stommel 1956). Similarly to Anderson and Corry (1985), the adjoint sensitivities indicate that the variations in the FC are largely sensitive to the wind stress in the western basin north of 26°N; however, on the analyzed time scale of 1 yr, the response is largely wind-generated baroclinic activity over topography. A summer maximum of the wind-generated baroclinic activity over topography, combined with a summer maximum of the fraction dependent on the curl of the wind stress, leads to the summer intensification of the FC transport (Anderson and Corry 1985). Although there is no improvement of representation of the summer intensification in the 1-yr experiments, it remains to be seen whether the weak

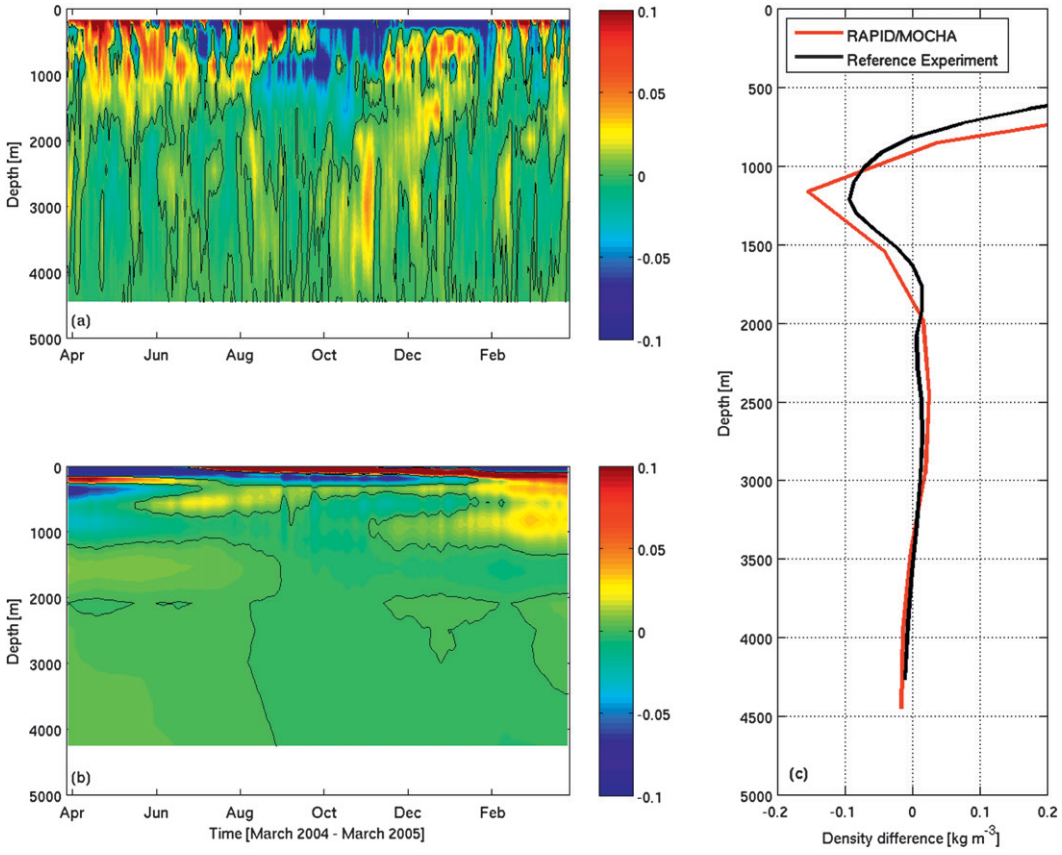

FIG. 4. Zonal density gradient (kg m^{-3}) between the eastern and western boundaries over first deployment period of RAPID–MOCHA: (left) Hovmöller diagram of daily anomalies for (a) observed and (b) reference experiment and (right) time-mean vertical profiles of zonal density gradient for observations (red line) and reference experiment (black line). The full zonal density gradient is the sum of both the time-mean vertical and the anomalies for each of the gradients.

seasonal cycle in the estimated FC transport can be improved through integration over longer periods of time in the full ECCO–GODAE solution.

To investigate the joint impact of the FC transport and the RAPID–MOCHA observations, we constrain the model to monthly-mean values instead of daily means, reducing the observation error to 0.5 Sv. Prior to that, we investigate the incorporation of the RAPID–MOCHA observations independent of the FC observations.

b. Moorings

One of the quantities that the deployed RAPID–MOCHA moorings readily deliver is the basinwide zonal density gradient. Before incorporating the RAPID–MOCHA data, we briefly compare the observed zonal density gradient to the reference experiment. Overall, the sign over the full water column is the same for both RAPID–MOCHA and the reference experiment (Fig. 4). The local minimum of the zonal density gradient near 1200 m is present in both RAPID–MOCHA and the reference experiment, although approximately 0.04 kg m^{-3} weaker in the reference experiment than in RAPID–MOCHA. The temporal variability in the zonal density gradient is dominated by high-frequency fluctuations in RAPID–MOCHA, while in the reference experiment the seasonal time scale dominates above 1000 m (Fig. 4). Note that for the full ECCO–GODAE, the sign of the time-mean zonal density gradient is generally the same as in the RAPID–MOCHA above 2000 m but different below 2000 m (Baehr et al. 2007). The absolute difference between RAPID–MOCHA and the full ECCO–GODAE in the time-mean zonal density gradient is largest near 1200 m (approximately 0.1 kg m^{-3}).

1) EXPERIMENTS

To investigate how the incorporation of the temperature and salinity observations of the RAPID–MOCHA affects the 1-yr experiments, we conduct some experiments in which the RAPID–MOCHA data are considerably upweighted. An experiment where the RAPID–MOCHA

data are not upweighted is described when combining both the FC and RAPID–MOCHA data.

In the first experiment (''daily RAPID''), we use daily observations of one merged profile of temperature and salinity at both the eastern and western boundaries. For this experiment, we upweight the RAPID–MOCHA data relative to every other observation by a factor of 100 (corresponding to 5% contribution to the total cost function). Here, we aim to upweight as strongly as possible, but larger factors result in unstable solutions. The data are weighted using the uncertainties derived by Forget and Wunsch (2007), which are based on a variety of in situ data, but excluding moorings. The variability of the daily RAPID–MOCHA time series is at several depths larger than the variances given by Forget and Wunsch (2007); however, Forget and Wunsch (2007) suggest that the high-frequency variability represents largely noise, while the low-frequency variability is most relevant for large-scale optimizations. We therefore average the daily RAPID–MOCHA time series to monthly data to reduce the amplitudes of the high-frequency variability. For the monthly-mean values, most of the observed variability is for both temperature and salinity at both the eastern and the western boundaries within the range of uncertainties given by Forget and Wunsch (2007) for the respective location.

In the second experiment (''monthly RAPID''), we reduce the temporal resolution to monthly means. To enhance the effect of the RAPID–MOCHA data in this experiment, we upweight the merged profiles of temperature and salinity at each of the eastern and western boundaries by a factor of 10.

Both experiments are run for six iterations. In the following, we describe the results of these two experiments and two additional experiments described later. We refer to them by their short name (as given in parentheses in this subsection) or commonly as RAPID experiments.

2) RESULTS

Relative to the reference experiment, the two experiments result in similar temperature and salinity adjustments with respect to the vertical structure (not shown). For temperature at both the eastern and western boundaries, the difference in the time-mean values between the two RAPID experiments and the observations is larger than the spread of the daily and monthly RAPID experiments at all depths. For salinity, the overall picture is less uniform, partly because the differences between the observations and the reference experiment are small from the start and partly because the different experiments result in slightly different solutions. Consequentially, the difference between the time-mean observed zonal density gradient and the daily and monthly RAPID experiments is larger than the spread shown by the two RAPID experiments (Fig. 5a). From the zonal density gradient, we derive thermal wind transports with a reference level at 4800 m and a spatially constant correction balancing the FC and the Ekman transport to ensure zero net mass transport across the section, similar to other databased approaches and similar to RAPID–MOCHA (Cunningham et al. 2007; Kanzow et al. 2007). Time-mean thermal wind transports (Fig. 5b) largely resemble the full meridional transports (Fig. 5c), except for depths below the Mid-Atlantic Ridge across which thermal wind has not been calculated, and the Antarctic Bottom Water is not resolved by the thermal wind transport either.

Overall, it is mostly the range between 2000 and 3000 m where both the density at the eastern and western boundaries (and in turn the zonal density gradient) have been improved in the optimized state estimate compared with the reference state estimate (Fig. 5). At other depths, either only the eastern boundary (generally above 1000 m) or only the western boundary (generally below 3000 m) shows improvement.

For the intermediate layer transport, the meridional transport derived from the RAPID–MOCHA is generally northward, while transports in the 1-yr experiments vary around zero (Fig. 5). Note that the full ECCO–GODAE transport in this layer is always southward. As the analysis of temperature and salinity suggests, neither the daily nor the monthly RAPID experiments result in a considerable adjustment of the zonal density gradient at intermediate depths (Fig. 5d). Note that at these intermediate depths the adjustments in the thermal wind transport in the RAPID experiments relative to the thermal wind transport in the reference experiment (Fig. 5e) are largely due to an adjustment of the transport at the reference level, with little influence on the total meridional transport (Fig. 5f).

For the upper North Atlantic Deep Water (NADW) transport, both the daily and the monthly RAPID experiments exhibit an adjustment in the mean strength of the meridional transport (Fig. 5f), which sums to approximately 1 Sv when integrating over this upper NADW layer. In terms of the hydrographic characteristics, at the western boundary this represents a cooling of up to 0.1°C at 1000 m and a warming of 0.05°C between 1500 and 3000 m (not shown). At the eastern boundary, it represents only small adjustments in temperature at 1000 m but a warming of up to 0.05°C between 1500 and 2000 m in both RAPID experiments. Changes in salinity at the eastern boundary are small and not uniform across the two RAPID experiments, although predominantly a freshening occurs with respect to the reference experiment

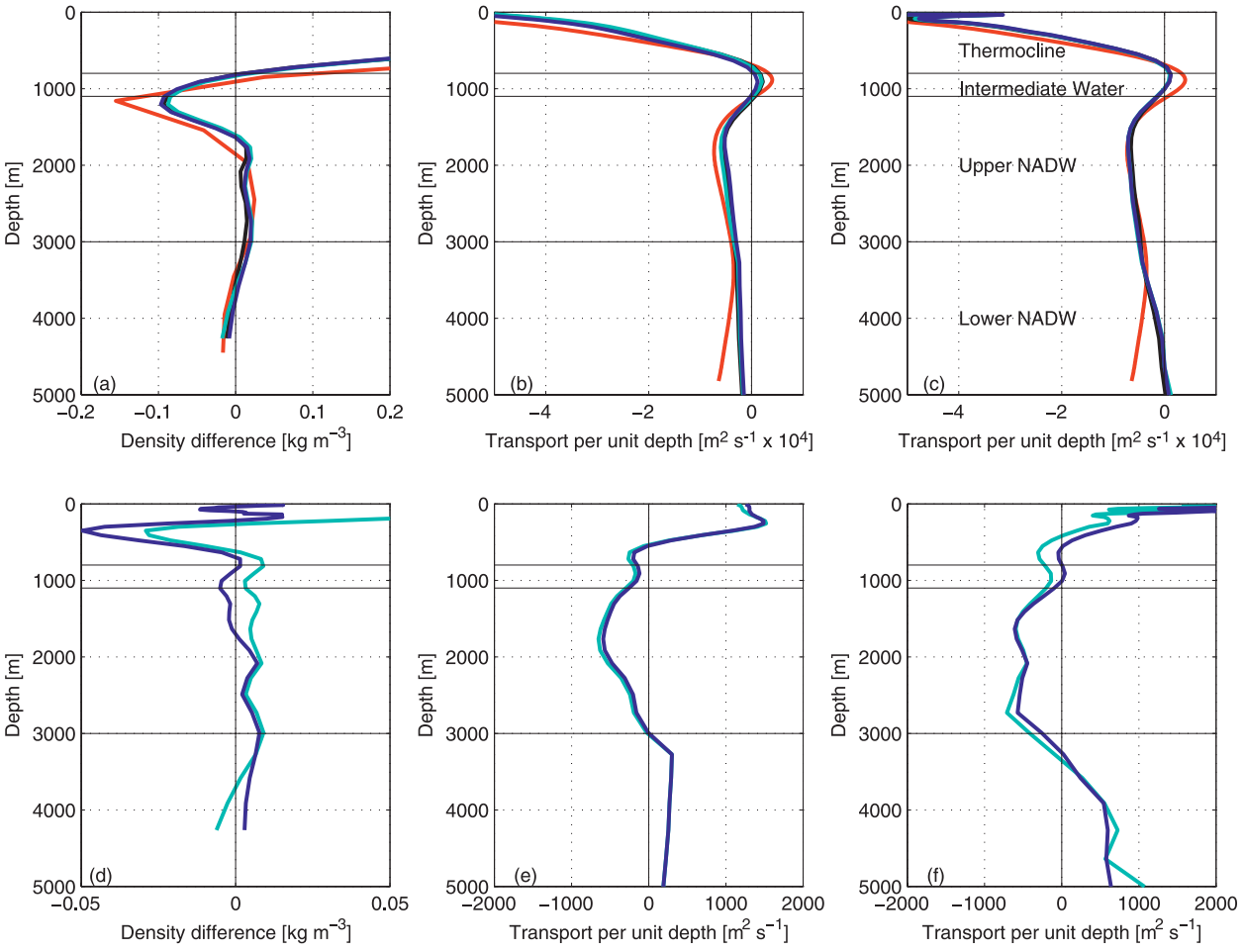

FIG. 5. (top) Time-mean (a) zonal density gradient, (b) resulting thermal wind transport (reference level at 4800 m), and (c) vertical profiles of meridional transport for observations (red lines), reference experiment (black lines), daily RAPID experiment (cyan lines), and monthly RAPID experiment (blue lines). (bottom) Difference of the two RAPID experiments minus the reference experiment for (d) zonal density gradient, (e) thermal wind transport, and (f) meridional transport. Units for (a),(d) are kg m^{-3} and for (b),(c),(e),(f) are m^2 s^{-1}.

above 2000 m, while water becomes more saline below (not shown). In turn, for the zonal density gradient this salinity change results in a slightly stronger negative density gradient between 1000 and 1600 m and a slightly stronger positive density gradient between 1600 and 2500 m with respect to the reference experiment (Fig. 5d). The gradient difference, in turn, results in larger thermal wind transports between 1000 and 2500 m in the two RAPID experiments compared to the reference experiment (Figs. 5e,f).

Integrated over the four depth layers indicated in Fig. 5, the magnitude of the temporal variability of the 14-day running mean smoothed meridional transport is at most depths comparable to the magnitude of variability shown by the transport derived from the RAPID–MOCHA (not shown). However, apart from the upper thermocline, correlations between the transports derived from the RAPID experiments and the transports derived from the RAPID–MOCHA are small and generally not significant.

Changes in the daily and monthly RAPID experiments with respect to the reference experiment are very similar throughout the Atlantic basin considering both the MOC (Figs. 6a,b) and the vertically integrated transport (not shown). Changes in the time-mean MOC are up to 2 Sv, occur mostly at lower depths (below 2000 m), and are confined to the direct vicinity mostly south of 26°N (±5°; Figs. 6a,b). Smaller adjustments (up to 1 Sv) spread well into the North Atlantic, weakening the comparatively deep MOC cell (both apparent in the one-year setup as well as in ECCO–GODAE). Changes in the vertically integrated meridional transport indicate an increase in the western boundary transport east of the Bahamas at 26°N and a recirculation at adjacent northern latitudes.

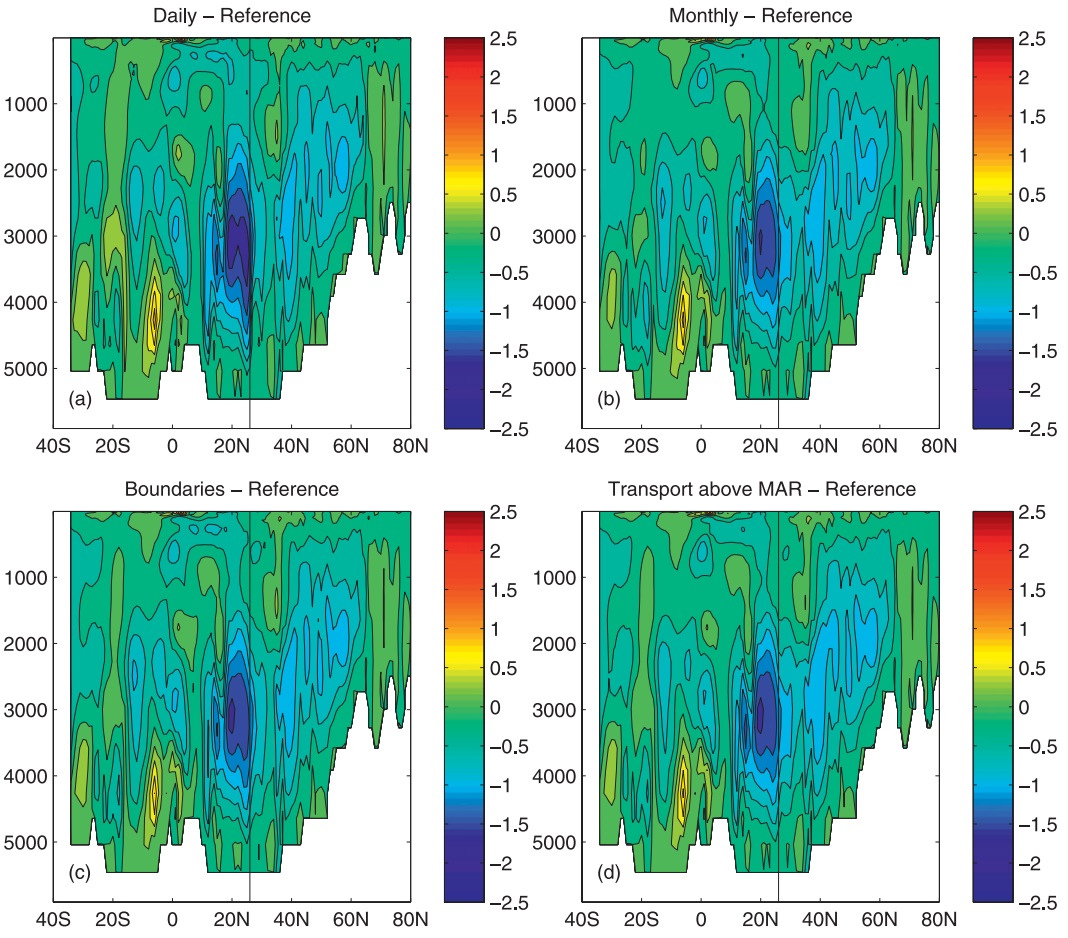

FIG. 6. Time-mean Atlantic MOC (Sv) for RAPID experiments minus reference experiment: (a) daily RAPID experiment, (b) monthly RAPID experiment, (c) boundaries RAPID experiment, and (d) transport-above-MAR RAPID experiment.

3) ADDITIONAL EXPERIMENTS

To test whether these patterns are dynamically robust, we perform two additional experiments: (i) in a "boundaries" experiment, we use the monthly-mean observations, but instead of using a single merged temperature and salinity profile on each the eastern and western boundaries, we put the profile at multiple adjacent locations to fill the entire eastern and western boundaries, respectively. For this experiment, the RAPID–MOCHA observations are upweighted by a factor of 100. (ii) In a "transport-above-MAR" experiment, we constrain the basinwide integrated transport above the crest of the MAR (i.e., above 3000 m), to the transport derived from the RAPID–MOCHA by Cunningham et al. (2007). We use monthly-mean values with an observation error of 1 Sv and additionally upweight this transport by a factor of 10^4 (resulting in more than 70% contribution of the transport term to the total cost function). With the boundaries experiment, we expect to understand whether the merged profiles at the eastern and western boundary profiles are representative for the entire boundary (i.e., representing the full zonal density gradient). With the transport-above-MAR experiment, we test whether the assumptions made to derive the transport estimate for the RAPID–MOCHA and the model dynamics used to derive the transport estimate in our model setup are compatible.

Both the boundaries experiment and the transport-above-MAR experiment result in a similar adjustment in the Atlantic MOC (Figs. 6c,d) as the monthly RAPID experiment. Also, the vertically and zonally integrated flow indicates the same patterns for the entire Atlantic in the boundaries experiment, the transport-above-MAR experiment, and the monthly RAPID experiment (not shown). This similarity in the four RAPID experiments indicates a dynamically robust influence of the RAPID–MOCHA moorings on the 1-yr experiments.

It also suggests that the dynamical assumptions used by Cunningham et al. (2007) to calculate the midocean transport (i.e., thermal wind and a spatially uniform mass balance correction) yield similar results as the assumptions used in the model.

Note that the RAPID experiments were set up differently both with respect to the quantity constrained to and the relative weight/upweighting given to the RAPID–MOCHA data and the transport derived from them, respectively. Apart from the transport-above-MAR experiment, the RAPID experiments use the same set of uncertainties in the vertical (following Forget and Wunsch 2007). Using smaller uncertainties results in strong adjoint sensitivities to a fraction of the RAPID–MOCHA data and in turn limited representativeness of the solution. In the following, we therefore use no upweighting and the uncertainties derived by Forget and Wunsch (2007) in conjunction with monthly averaged merged profiles at the eastern and western boundaries, because the daily resolution of the RAPID–MOCHA data is too high to be fully represented by the model.

c. *Combined experiment*

We use the monthly-mean FC observations (with an observation error of 0.5 Sv) and the monthly-mean RAPID–MOCHA observations of temperature and salinity and the eastern and western boundaries of 26°N [using Forget and Wunsch (2007) uncertainties and no upweighting] to investigate the joint impact of both datasets (''combined'' experiment). We integrate this experiment for 15 iterations and compare it to the same number of iterations as the reference experiment. At this point, the reduction in the cost functions for both the FC and RAPID–MOCHA data is less than 2% for two subsequent iterations.

At 26°N, the adjustments in the combined experiment are largely an overlay of both the monthly FC experiment and the monthly RAPID experiment. An increase in the FC transport seen in both experiments (2.6 Sv in the monthly FC experiment and 0.6 Sv in the monthly RAPID experiment) is mirrored in a larger FC transport by 3.8 Sv in the combined experiment (Fig. 7a). With a standard deviation of 2.5 Sv in the combined experiment, the variability is unadjusted with respect to the reference experiment. These adjustments in the FC transport are not entirely mirrored in the MOC at 26°N. With 16.0 Sv, the time mean of the maximum of the MOC at 26°N is slightly smaller for the combined experiment than for the experiment constrained to the monthly FC observations (16.3 Sv) but larger compared to the reference experiment (15.1 Sv) and the monthly RAPID experiment (15.0 Sv; Fig. 7b). Overall, the high-frequency MOC variability at 26°N is mostly wind driven (cf. Baehr et al. 2007), and the high-frequency variability is reproduced quite realistically already prior to the assimilation of the FC and RAPID–MOCHA. Basinwide transports (outside the FC and below the Ekman layer), however show little correlation between the observations and the assimilated experiments.

At 26°N, adjustments in the MOC are small compared to the adjustments in both the northward and southward transports; partly, these transport adjustments compensate for each other, but the increase in the FC transport is also balanced by a local recirculation. Changes in the variability of the MOC are also small at 26°N. The standard deviation of the maximum MOC time series at 26°N is 4.3 $\pm$ 0.1 Sv for all four experiments. While the strongest effect of the FC data is seen in the northward transport, the effect of the RAPID mooring data is seen in the time-mean midocean geostrophic transport (Fig. 7c). In the intermediate water, the differences to the RAPID–MOCHA midocean transport derived by Cunningham et al. (2007) are larger, mostly similar—albeit a bit weaker—to the adjustments seen in the monthly FC experiment. In the upper NADW, the differences to the RAPID–MOCHA midocean transport are smaller, mostly similar to the adjustments seen in the monthly RAPID experiment.

Changes in the time-mean Atlantic MOC and the North Atlantic heat transport with respect to the reference experiment are more prominent away from 26°N (Figs. 7d,e). North of 26°N, both the time-mean MOC and the meridional heat transport are larger from 26°N to near 40°N with respect to the reference experiment, largely similar to the adjustments seen in the monthly FC experiment. The time-mean MOC is larger by approximately 1 Sv, and the time-mean meridional heat transport is larger by 0.05 PW with respect to the reference experiment. South of 26°N, the deep limb of the MOC is larger by approximately 0.8 Sv at 3000 m, largely similar to the adjustments seen in the monthly RAPID experiment. Note that these adjustments spread from 26°N well into the South Atlantic (Fig. 7d) but no longer north of 26°N as in the RAPID experiments. Adjustments in the heat transport, however, are dominated by the adjustments resulting from the incorporation of the FC data, because the RAPID–MOCHA data largely result in a restructuring of the deep flow, with an overall (weak, order 0.1 Sv) reduction in the MOC and little impact on the MHT in the combined experiment.

4. Discussion and conclusions

Here, we test strategies of incorporating both FC transport observations and RAPID–MOCHA temperature and salinity observations for March 2004–March 2005

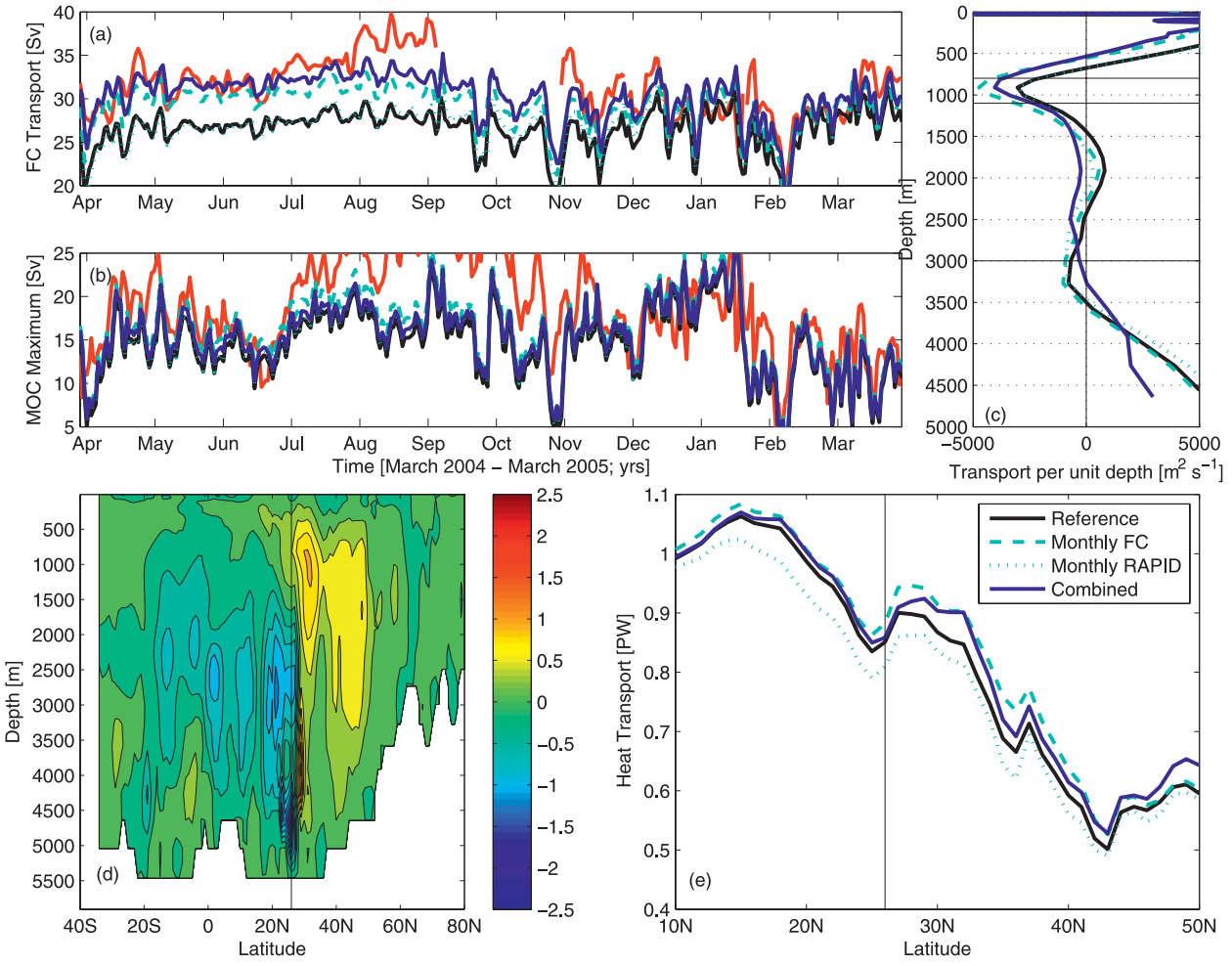

FIG. 7. Results from the combined experiment: (a) time series of FC transport (Sv), (b) time series of MOC maximum (Sv) at 26°N, (c) time-mean midocean geostrophic transport difference to RAPID–MOCHA midocean transport (m^2 s^{-1}) by Cunningham et al. (2007), (d) time-mean MOC (Sv) for combined experiment minus reference experiment, and (e) time-mean North Atlantic meridional heat transport (PW). The following are represented by colored lines in (a)–(c),(e): observations (red), reference experiment (black), monthly FC experiment (dashed cyan), monthly RAPID experiment (dotted cyan), and combined experiment (blue).

into an experimental 1-yr setup of the ECCO–GODAE setup. The optimized solution is compared to a reference experiment, an identical setup with the exception of the RAPID–MOCHA and FC data. For the FC data, we find that the optimization is sensitive to the time mean, whereas the variability remains largely unadjusted compared with the reference experiment. For the mooring data, we find the incorporation of monthly-mean data to be robust when including the mooring data as single profiles at the boundaries, when including them as repeated profiles covering the entire boundary and also when constraining to the transport derived from thermal wind using the moored time series of temperature and salinity. Using both the FC and RAPID–MOCHA data as an observational constraint results in a larger MOC and heat transport between 26° and 40°N, with a maximum near 30°N in the 1-yr experiments. The results of the present study suggest that the integrated transport across the Florida Straits should be incorporated on a monthly (rather than daily) basis and that the RAPID mooring data should also be incorporated on a monthly (rather than daily) basis and weighted with the uncertainties of Forget and Wunsch (2007) derived from in situ data.

The similarity in the four RAPID experiments indicates a dynamically robust—albeit upweighted—influence of the RAPID–MOCHA moorings on the 1-yr experiments. In the combined experiment, where the RAPID data are not upweighted, this influence seems to be mirrored in a larger southward transport in the upper NADW. Some of this southward transport and also some of the larger northward transport resulting from the FC data appear to recirculate locally, suggesting that

the model is adjusting locally rather than on a large scale. Note that, with a higher number of iterations for the combined experiment (15 compared to approximately 5 for the separate tests), this effect is somewhat reduced, especially for the influence of the RAPID–MOCHA moorings.

The incorporation of the FC and RAPID–MOCHA data is subject to limitations. Despite strong constraints, some discrepancies between the observed and modeled hydrographic characteristics remain with respect to both time-mean values and variability. For example, the optimization appears insensitive to some of the largest discrepancies between the RAPID–MOCHA data and the reference experiment (e.g., the 0.5°C time-mean temperature discrepancy at 1000 m at the western boundary). Also, the temporal variability of the basinwide transports (i.e., without the FC and below the Ekman layer) is largely unaffected by the assimilation of the RAPID–MOCHA data. The most prominent inherent limitation is the spatial resolution, which results in a limited representation of the spatiotemporal variability in the model. The RAPID–MOCHA measurements represent local time series with a high temporal and vertical resolution with a considerable contribution of eddy noise (Wunsch 2008). It is therefore not straightforward to assume that these local measurements are representative for grid boxes of 100 km $\times$ 100 km. For the limited horizontal resolution, we find that the monthly averaged data are within the hydrographic uncertainties estimated by Forget and Wunsch (2007). The incorporation of the monthly data results in dynamically stable results for a local or boundary constraint of temperature and salinity profiles or a basinwide integrated transport constraint; however, it would be clearly desirable to test the robustness of these results in an eddy-resolving state estimate when it becomes available, ultimately also allowing to assimilate unsmoothed (daily) data. For the limited vertical resolution, some of the remaining differences between the RAPID mooring data and the 1-yr experiments in the vertical structure can be attributed to the limited vertical resolution (e.g., 0.5 Sv in the time mean for the mid-ocean geostrophic transport).

The incorporation of both the FC and the RAPID–MOCHA data result in adjustments of the meridional transport away from 26°N, suggesting that both adjustments in the FC transport at 26°N and adjustments in the zonal density at 26°N are intimately linked to adjustments in the MOC in the North Atlantic. Seasonal and interannual FC variability, however, does not reflect open ocean variability in the subtropical Atlantic (Schott and Zantopp 1985); time scales of a year and longer need to be considered to link open ocean and the FC variability. Whether the temporal variability of the FC on these time scales can be improved through the assimilation over longer periods remains therefore to be seen. Note that longer assimilation periods will also change the importance of the adjustments to the initial conditions (compared with the forcing). The sensitivity of the North Atlantic MOC to changes in the zonal density gradient in the subtropical Atlantic is in good agreement with the results by Marotzke et al. (1999). The continuous observation of zonal density gradients in the upper NADW layer has also been suggested to provide a timely detection of changes in the MOC at 26°N on decadal time scales and longer (Baehr et al. 2007). The continuous observation of both the FC and the zonal density contrast across 26°N is therefore an important step toward a comprehensive MOC monitoring system.

The adjustments we find in the 1-yr experiments with respect to the 1-yr reference experiment can neither in structure nor magnitude be expected to be found in perfect similarity in the full ECCO–GODAE solution. As shown for the FC data, the adjustment of the initial conditions plays a crucial role in the 1-yr experiments; however, it is not only that the actual initial conditions are different in the ECCO–GODAE solution, it is also that their optimization has less influence on the full 15-yr ECCO–GODAE integration. At 26°N, the hydrographic characteristics in the 1-yr experiments prior to the incorporation of both the FC and RAPID–MOCHA data are considerably closer to the RAPID–MOCHA observations than in ECCO–GODAE: for example, at intermediate waters at the western boundary where discrepancies between the RAPID–MOCHA and the ECCO–GODAE solution are largest (Baehr et al. 2009). While this means that it requires a larger adjustment in the ECCO–GODAE solution than in the 1-yr experiments to fit the RAPID–MOCHA data, the solution is also more sensitive to reduce a large misfit between model and observations than a small one. This also applies to misfits in the temporal variability (e.g., the high-frequency FC variability); however, the number of iterations needed to converge toward certain data is considerably larger in ECCO–GODAE, and adjustments in the solution resulting from the FC or RAPID–MOCHA data will evolve slowly over a considerable number of iterations. Note as well that the FC data are available for the full 15-yr time span, but the RAPID–MOCHA moorings are at present available for 1 yr only.

The incorporation of the FC and RAPID–MOCHA data for March 2004–March 2005 into an experimental 1-yr setup of ECCO–GODAE does not result in profound adjustments at 26°N or even in the North Atlantic circulation, as expected. While structure and magnitude of the adjustments have yet to be confirmed when integrating over longer periods of time, in the given model

and on the analyzed time scale of 1 yr, the results suggest the following:

- The incorporated transport measurements and transbasin mooring measurements result in regional circulation adjustments. These adjustments are in agreement with previously incorporated data but had not been achieved with them. Specifically, transport measurements and deep density gradients result in adjustments in the Gulf Stream transport and the NADW transport, respectively.
- The region of influence appears to be limited to 26°N and adjacent latitudes (approximately ±10°–15°), suggesting the need for additional boundary current measurements and deep zonal density gradient measurements throughout the Atlantic and/or their respective incorporation to further constrain the circulation.
- Further strategies for incorporating transport and mooring observations into a dynamically consistent state estimate such as ECCO–GODAE have to be tested to improve the representation of the monthly to seasonal variability of these data. Such a further improved representation will be crucial to initialize seamless to decadal predictions of the North Atlantic circulation and its variability.

Acknowledgments. I wish to thank Gaël Forget, Patrick Heimbach, Torsten Kanzow, and Carl Wunsch for stimulating discussions and for helpful comments on the manuscript. The two reviewers and the editor provided valuable comments on the manuscript. The RAPID–MOCHA mooring operations have been funded by the Natural Environment Research Council, RAPID, and NSF. The Florida Current cable data are made freely available by the Atlantic Oceanographic and Meteorological Laboratory (available online at http://www.aoml.noaa.gov/phod/floridacurrent/) and are funded by the NOAA Office of Climate Observations. ECCO–GODAE is supported by the National Ocean Partnership Program (NOAA, NASA, and NSF), with additional funding from NASA.

REFERENCES

Anderson, D. L. T., and R. A. Corry, 1985: Seasonal transport variations in the Florida Straits: A model study. *J. Phys. Oceanogr.,* **15,** 773–786.

Baehr, J., H. Haak, S. Alderson, S. A. Cunningham, J. Jungclaus, and J. Marotzke, 2007: Timely detection of changes in the meridional overturning circulation at 26°N in the Atlantic. *J. Climate,* **20,** 5827–5841.

——, K. Keller, and J. Marotzke, 2008: Detecting potential changes in the meridional overturning circulation at 26°N in the Atlantic. *Climatic Change,* **91,** 11–27, doi:10.1007/s10584-006-9153-z.

——, S. A. Cunningham, H. Haak, P. Heimbach, T. Kanzow, and J. Marotzke, 2009: Observed and simulated variability of the meridional overturning circulation at 26.5°N in the Atlantic. *Ocean Sci.,* **5,** 575–589.

Baringer, M. O., and J. C. Larsen, 2001: Sixteen years of Florida Current transport at 27°N. *Geophys. Res. Lett.,* **28,** 3179–3182.

Bryden, H. L., H. R. Longworth, and S. A. Cunningham, 2005: Slowing of the Atlantic meridional overturning circulation at 25°N. *Nature,* **438,** 655–657.

Cunningham, S. A., and Coauthors, 2007: Temporal variability of the Atlantic meridional overturning circulation at 26.5°N. *Science,* **317,** 935–938.

Forget, G., 2010: Mapping ocean observations in a dynamical framework: A 2004–06 ocean atlas. *J. Phys. Oceanogr.,* in press.

——, and C. Wunsch, 2007: Estimated global hydrographic variability. *J. Phys. Oceanogr.,* **37,** 1997–2008.

——, B. Ferron, and H. Mercier, 2008a: Combining Argo profiles with a general circulation model in the North Atlantic. Part 1: Estimation of hydrographic and circulation anomalies from synthetic profiles, over a year. *Ocean Modell.,* **20,** 1–16.

——, H. Mercier, and B. Ferron, 2008b: Combining Argo profiles with a general circulation model in the North Atlantic. Part 2: Realistic transports and improved hydrography, between spring 2002 and spring 2003. *Ocean Modell.,* **20,** 17–34.

Ganachaud, A., and C. Wunsch, 2000: Improved estimates of global ocean circulation, heat transport and mixing from hydrographic data. *Nature,* **408,** 453–457.

Giering, R., and T. Kaminski, 1998: Recipes for adjoint code construction. *ACM Trans. Math. Software,* **24,** 437–474.

Graf, J., C. Sasaki, C. Winn, W. T. Liu, W. Tsai, M. Freilich, and D. Long, 1998: NASA Scatterometer Experiment. *Acta Astronaut.,* **43** (7–8), 397–407.

Hall, M. M., and H. L. Bryden, 1982: Direct estimates and mechanisms of ocean heat transport. *Deep-Sea Res.,* **29A,** 339–359.

Heimbach, P., C. Hill, and R. Giering, 2005: An efficient exact adjoint of the parallel MIT general circulation model, generated via automatic differentiation. *Future Gener. Comput. Syst.,* **21,** 1356–1371, doi:10.1016/j.future.2004.11.010.

Kanzow, T., and Coauthors, 2007: Observed flow compensation associated with the MOC at 26.5°N in the Atlantic. *Science,* **317,** 938–941.

Köhl, A., and D. Stammer, 2008: Variability of the meridional overturning in the North Atlantic from the 50-yr GECCO state estimation. *J. Phys. Oceanogr.,* **38,** 1913–1930.

Larsen, J. C., 1985: Florida Current volume transports from voltage measurements. *Science,* **277,** 302–304.

Longworth, H. R., and H. L. Bryden, 2007: Discovery and quantification of the Atlantic meridional overturning circulation: The importance of 25N. *Ocean Circulation: Mechanisms and Impacts: Past and Future Changes of Meridional Overturning. Geophys. Monogr.,* Vol. 173, Amer. Geophys. Union, 5–18.

Marotzke, J., R. Giering, K. Q. Zhang, D. Stammer, C. Hill, and T. Lee, 1999: Construction of the adjoint MIT ocean general circulation model and application to Atlantic heat transport sensitivity. *J. Geophys. Res.,* **104,** 29 529–29 547.

——, S. A. Cunningham, and H. L. Bryden, 2002: Monitoring the Atlantic meridional overturning circulation at 26.5°N. Natural Environment Research Council. [Available online at http://www.noc.soton.ac.uk/rapidmoc/.]

Marshall, J., C. Hill, L. Perelman, and A. Adcroft, 1997: Hydrostatic, quasi-hydrostatic and nonhydrostatic ocean modeling. *J. Geophys. Res.,* **102** (C3), 5733–5752.

Meinen, C. S., S. L. Garzoli, W. E. Johns, and M. O. Baringer, 2004: Transport variability of the deep western boundary current

and the Antilles Current off Abaco Island, Bahamas. *Deep-Sea Res. I.,* **11,** 1397–1415.

Rayner, D., 2005: RRS Discovery cruise D277/D278 RAPID mooring cruise report February–March 2004. Southampton Oceanography Centre Tech. Rep., 103 pp.

Roemmich, D., and C. Wunsch, 1985: Two transatlantic sections: Meridional circulation and heat flux in the subtropical North Atlantic Ocean. *Deep-Sea Res.,* **32,** 619–664.

Schott, F., and R. Zantopp, 1985: Florida Current: Seasonal and interannual variability. *Science,* **227,** 308–311.

Veronis, G., and H. Stommel, 1956: The action of variable wind stresses on a stratified ocean. *J. Mar. Res.,* **15,** 43–75.

Wunsch, C., 2008: Mass and volume transport variability in an eddy-filled ocean. *Nat. Geosci.,* **1,** 165–168, doi:10.1038/ngeo126.

——, and P. Heimbach, 2006: Estimated decadal changes in the North Atlantic meridional overturning circulation and heat flux 1993–2004. *J. Phys. Oceanogr.,* **36,** 2012–2024.

——, and ——, 2007: Practical global oceanic state estimation. *Physica D,* **230,** 197–208.